Dovepress

Open Access Full Text Article

ORIGINAL RESEARCH

Zinc oxide nanoparticles induce toxic responses in human neuroblastoma SHSY5Y cells in a size-dependent manner

Jia Liu[1]
Yiyuan Kang[1]
Suhan Yin[1]
Bin Song[2]
Limin Wei[3]
Liangjiao Chen[4]
Longquan Shao[1]

[1]Department of Stomatology, Nanfang Hospital, Southern Medical University, Guangzhou, [2]Department of Stomatology, Guizhou Provincial People's Hospital, Guiyang, [3]Department of Pediatric Dentistry, School and Hospital of Stomatology, Wenzhou Medical University, Wenzhou, [4]Key Laboratory of Oral Medicine, Guangzhou Institute of Oral Disease, Stomatology Hospital of Guangzhou Medical University, Guangzhou, China

Correspondence: Longquan Shao
Department of Stomatology, Nanfang Hospital, Southern Medical University, 1838 Guangzhou North Avenue, Baiyun Qu, Guangzhou, Guangdong 510515, China
Tel +86 159 8928 3921
Email shaolongquan@smu.edu.cn

Abstract: Due to the widespread applications of zinc oxide nanoparticles (ZnO NPs), the potential exposure of workers, consumers, and scientists to these particles has increased. This potential for exposure has attracted extensive attention in the science community. Many studies have examined the toxicological profile of ZnO NPs in the immune system, digestive system, however, information regarding the toxicity of ZnO NPs in the nervous system is scarce. In this study, we detected the cytotoxicity of two types of ZnO NPs of various sizes – ZnO[a] NPs and ZnO[b] NPs – and we characterized the shedding ability of zinc ions within culture medium and the cytoplasm. We found that reactive oxygen species played a crucial role in ZnO NP-induced cytotoxicity, likely because zinc ions were leached from ZnO NPs. Apoptosis and cytoskeleton changes were also toxic responses induced by the ZnO NPs, and ZnO[b] NPs induced more significant toxic responses than ZnO[a] NPs in SHSY5Y cells. In conclusion, ZnO NPs induced toxic responses in SHSY5Y cells in a size-dependent manner, which can probably be attributed to their ion-shedding ability.

Keywords: zinc oxide, nanoparticles, SHSY5Y cells, reactive oxygen species, apoptosis, cell cytoskeleton

Introduction

The use of engineered nanoparticles (NPs) has increased, because their application in various fields, such as electronics, biomedicine, pharmaceuticals, cosmetics, energy applications, and materials, has expanded rapidly during the past few decades.[1] Meanwhile, their toxic side effects are increasing daily. Recently, various investigators have striven to elucidate the deleterious effects of these nanomaterials.[2,3] Some of these NPs, such as silver, titanium dioxide (TiO_2) and zinc oxide NPs (ZnO NPs), which are widely detected in living environments, drinking water, and various consumer products, have been reported to induce inflammation, oxidative stress, and cytotoxicity.[2,4] ZnO NPs have been widely used in drug delivery, the pharmaceutical industry, biomedical engineering, sunscreens, food additives, and cosmetics.[5] Due to the large increase in the prevalence of nanomaterials, the potential of increased exposure exists for consumers, industry workers, and hence more research should be performed to mitigate their toxic side effects.

ZnO NPs show higher toxic effects than other metallic oxide NPs, such as TiO_2,[6–8] likely because of their ion-shedding ability. ZnO NPs exhibit low solubility under neutral conditions, but are readily soluble under acidic conditions, such as in lysosomes.[9,10] This behavior is similar to that of other soluble metallic NPs, such as silver.[11,12] However, when

compared with ZnO NPs, silver exhibits lower solubility in acidic conditions and higher solubility in neutral conditions.[9,11] The principal neurotoxic mechanism of ZnO NPs is the mass production of reactive oxygen species (ROS) via the disturbance of metal-ion homeostasis due to an intracellular increase in dissolved free zinc ions.[13,14] Elevated levels of zinc ions are considered the major contributor to ZnO NP-induced cytotoxicity, causing oxidative stress[3] and inflammation.[15]

Various studies have shown that ZnO NPs with various shapes, such as rods and spheres, probably cause neurotoxicity due to their ability to access the brain.[16–18] Moreover, the olfactory brain route has also been reported as a potential route for ZnO NPs transfer into the brain.[19] However, information regarding the neurotoxic effects of ZnO NPs is scarce. Therefore, understanding the effects of nanomaterial exposure, including neurotoxicity, is important for ensuring the safety of nanomaterials, particularly when the particles are used in biomedical applications. Cytotoxicity severity has been shown to depend on the physicochemical properties of the NPs, such as chemical composition, size, shape, aggregation, surface chemistry, and surface energy.[20–23] The physicochemical characteristics of NPs, such as being sufficiently small to penetrate the blood–brain barrier, and their large surface area can promote their neurotoxicity.[24]

Therefore, we aimed to investigate the toxic effects of ZnO NPs in neuronal SHSY5Y cells by assessing their cytotoxic effects, oxidative stress, apoptotic damage, and morphological changes under in vitro conditions. Meanwhile, we discuss the toxic effects of two types of ZnO NPs with different physicochemical properties and investigate the role of zinc ions in ZnO NP-induced toxic effects.

Materials and methods
Chemicals
ZnO[a] NPs were purchased from Sigma-Aldrich (677450; St Louis, MO, USA), as were ZnO[b] NPs (544906) and zinc chloride (ZnCl$_2$; Z0152). FBS, DMEM, FluoZin-3 AM, LysoTracker Red DND-99, Hoechst 33342, and Alexa Fluor 594 phalloidin were purchased from Thermo Fisher Scientific (Waltham, MA, USA). The monoclonal anti-α-tubulin antibody was purchased from Sigma-Aldrich. NPs were dispersed by probe sonication for 120 minutes in PBS to yield a stock solution of 1 mg/mL. All other reagents were of the highest purity, commercially available, and used as received.

Concentration of dissolved zinc in cell-culture medium
ZnO NP suspensions (0, 5, 10, 25, 50, 75, and 100 μg/mL) were prepared using complete culture medium and incubated for

24 hours at 37°C. The suspensions were then centrifuged at 20,000 rpm for 30 minutes. Supernatants were then transferred into 1.5 mL centrifuge tubes for analysis. Zinc content was detected using an inductively coupled plasma mass spectrometry (X-Series 2; Thermo Fisher Scientific).

SHSY5Y cell cultures and differentiation
The human neuroblastoma SHSY5Y cell line was obtained from the cell bank of the Shanghai Infrastructure for Public Research and Development of the Chinese Academy of Medical Sciences. DMEM supplemented with 10% FBS and 1% penicillin–streptomycin (Thermo Fisher Scientific) was used for SHSY5Y cell culture, and the cells were incubated at 37°C with 5% CO$_2$. The culture medium was replaced every other day, and cells were passaged when confluence reached 80%–90%. To obtain cells with neuronal phenotypes, we attempted to induce differentiation in SHSY5Y cells using trans-retinoic acid, and we observed morphology changes at 0, 3, 6, 9, 12, and 15 days.

To investigate the biological effects of the ZnO NPs, SHSY5Y cells were incubated in a complete culture medium for 24 hours before the addition of the ZnO NPs at various concentrations. The ZnO NPs were diluted to 100 μg/mL from a stock solution of 1 mg/mL, dispersed for 30 minutes with a sonicator to prevent aggregation, and then diluted to the specified concentrations for treating the cells. We list the relative relationships between the different concentrations of the ZnO NPs and ZnCl$_2$ in Table 1.

Cell-proliferation assays after ZnO NP and ZnCl$_2$ treatments
Cellular viability was determined using the CCK-8 assay (Dojindo Molecular Technologies, Kumamoto, Japan). Cells were seeded in each well in 96-well plates with 5,000 cells/well. Then, 100 μL of the complete culture medium was added per well and cells incubated for 24 hours at 37°C. The ZnO NPs were then added to the 96-well plates at concentrations of 5, 10, 20, 40, 60, 80, and 100 μg/mL, and ZnCl$_2$ was added at concentrations of 61.4, 122.9, 245.7, 491.5, 737.2, 982.9, and 1,228.7 μM. The plates were incubated for 2, 6, 12, or 24 hours

Table 1 Relative relationship between ZnO NPs and ZnCl$_2$ at different concentrations

Type of particle	Concentration						
Zinc element (μM)	61.4	122.9	245.7	491.5	737.2	982.9	1,228.7
Zinc element (μg/mL)	4.02	8	16.1	32.1	48.2	64.3	80.33
ZnO (μg/mL)	5	10	20	40	60	80	100
ZnCl$_2$ (μg/mL)	8.37	16.75	33.5	67	100.5	134	167.46

Abbreviation: NPs, nanoparticles.

at 37°C. The control group was untreated. Finally, detection reagents were added to each well, and the 96-well plates were then incubated for an additional 2 hours at 37°C. To prevent the NPs from interfering in this analytical assay, an empty 96-well plate was prepared and the solution from each well quantitatively transferred to the empty plate. Subsequently, absorbance was measured using a microplate reader at a wavelength of 450 nm. Six replicates were performed for each treatment. Moreover, N-acetyl-L-cysteine (NAC), an ROS scavenger, was used to detect the role of ROS in the ZnO NP-induced toxic response. SHSY5Y cells were incubated with the ZnO NPs or $ZnCl_2$ for 24 hours, accompanied by NAC (10 mM), and then cells were evaluated as previously described.

Confocal study of zinc ion-release process after ZnO NP treatment

The human neuroblastoma SHSY5Y cell line was treated with 50 µg/mL of the ZnO NPs for 1, 3, or 5 hours. After treatment, cells were loaded with 3 µM FluoZin-3 at 37°C for 60 minutes. The cells were then washed twice with PBS and incubated with the culture medium at 37°C for 30 minutes to enable complete penetration of the fluorescence probe. Then, the culture medium was removed, and cells were loaded with 70 nM LysoTracker red DND-99 at 37°C for 1 hour. Finally, cell nuclei were loaded with Hoechst 33342 at 37°C for 20 minutes. Before fluorescence was observed, cells were washed twice with PBS and sealed with an antifade mounting medium (Beyotime, Haimen, China). All fluorescence measurements were obtained under confocal microscopy (FV10i; Thermo Fisher Scientific).

ROS-level detection in SHSY5Y cells after ZnO NP exposure

The formation of intracellular ROS was determined using an ROS-assay kit (Beyotime). Briefly, after being washed with PBS, 2×10^5 cells were seeded per well in a six-well plate at a volume of 2 mL. Then, cells were treated with two types of ZnO NPs at a concentration of 25 µg/mL for 1, 6, 12, and 24 hours or at a concentration of 50 µg/mL for 1, 3, and 5 hours. $ZnCl_2$ was used to analyze the toxic effects of the zinc ions in ZnO NP supernatants. After treatment with ZnO NPs and $ZnCl_2$, cells were collected and incubated with 10 µM dichlorodihydrofluorescein diacetate for 30 minutes at 37°C and 5% CO_2. Then, fluorescence intensity was analyzed using a FACSAria III (BD, Franklin Lakes, NJ, USA).

Cell-apoptosis detection via annexin V–FITC/PI detection assay

Annexin V–fluorescein isothiocyanate (FITC) and propidium iodide (PI) assays (Thermo Fisher Scientific) were conducted to detect cell apoptosis. The annexin V–FITC assay consists of an FITC-conjugated annexin V antibody that has a high affinity for membrane phosphatidylserine. In normal viable cells, the phosphatidylserine is located on the inner side of the cell membrane. Then, the phosphatidylserine flips and becomes exposed on the outer side of the plasma membrane upon activation of the cell-apoptosis pathway. This behavior can be used to detect the early apoptosis of cells. In addition, cells were incubated with PI, which cannot penetrate the cell membranes of viable cells or cells in an early apoptotic phase, and then cell nuclei were stained. However, PI can stain nuclei via penetrating the cell membranes of necrotic cells and cells in a late apoptotic phase. Using both dyes in combination with two-wavelength flow cytometry, apoptotic and necrotic cells were identified separately. Following 5 hours of incubation with different concentrations of ZnO NPs (0, 20, 40, and 60 µg/mL), cells were washed and stained with annexin V and PI. SHSY5Y cells were resuspended in 100 µL binding buffer and 5 µL FITC-conjugated annexin V, and 5 µL PI was added sequentially at room temperature in the dark. After 15 minutes of incubation, stained cells were diluted with 400 µL binding buffer and analyzed directly using the FACSAria.

RNA extraction and RT-PCR

Total RNA was extracted using Trizol reagent (Thermo Fisher Scientific), and RNA concentration was detected using ultraviolet spectrophotometry. Then, RNA was reverse-transcribed to cDNA using a reverse-transcription (RT) reagent kit (Takara Bio, Dalian, China). Real-time polymerase chain reaction (PCR) was conducted using SYBR green (Takara Bio). Several genes were detected: *SOD1*, *SOD2*, *CAT*, *GPX1*, *BAX*, *BCL2*, and *CYTC*. Data were analyzed using the $2^{-\Delta\Delta CT}$ method. The primers used are listed in Table 2.

Confocal study of cytoskeleton changes after ZnO NP treatment

The human neuroblastoma SHSY5Y cell line was treated with 50 µg/mL ZnO NPs for 1, 3, or 5 hours. After treatment, cells were treated with 4% paraformaldehyde for 20 minutes. Cells were then washed twice with PBS and treated with 1% Triton for 10 minutes. Then, cells were blocked via 5% BSA at 37°C for 1 hour and subsequently incubated with the monoclonal anti-α-tubulin antibody overnight at 4°C. Cells were washed three times for 10 min each with PBS. Afterward, cells were loaded with FITC-bound secondary antibody at 37°C for 1 hour. Additionally, cells were loaded with phalloidin, which can bind actin, at 37°C for 1 hour. Finally, cell nuclei were stained with Hoechst 33342 at 37°C

Table 2 Primers used for polymerase chain reaction

Gene	Forward	Reverse
SOD1	5′-CAGTGCAGGTCCTCACTTTA-3′	5′-CCTGTCTTTGTACTTTCTTC-3′
SOD2	5′-GGACAAACCTCAGCCCTAAC-3′	5′-TTGAAACCAAGCCAACCC-3′
CAT	5′-AGGGGCCTTTGGCTACTTTG-3′	5′-ACCCGATTCTCCAGCAACAG-3′
GPX1	5′-AGAACGCCAAGAACGAAGAG-3′	5′-ACAGGACCAGCACCCATCT-3′
BAX	5′-CCAGCTGCCTTGGACTGTGT-3′	5′-GGTTTATTACCCCCTCAAGACCAC-3′
BCL2	5′-GGTGAACTGGGGGAGGATTG-3′	5′-GACAGCCAGGAGAAATCAAACAG-3′
CYTC	5′-GCCCCTGGATACTCTTACAC-3′	5′-TCTGCCCTTTCTTCCTTCT-3′

for 20 minutes. Before fluorescence observation, cells were washed twice with PBS and sealed with an antifade mounting medium. All fluorescence measurements were obtained under confocal microscopy (FV10i).

Statistical analysis

Results are represented as means ± SEM. All data were assessed by analysis of variance. The homogeneity-of-variance test was performed, and Bonferroni and Dunnett's T3 tests were used when equal variance was assumed and there was no homogeneity, respectively. $P<0.05$ was considered significant.

Results
Characterization of ZnO NPs

Prior to biological testing, we characterized ZnO NP powders via transmission electron microscopy and dynamic light scattering. Transmission electron-microscopy data were used to determine particle shapes and sizes. ZnO[a] NPs were irregular and rod-shaped with smooth surfaces, average size was 47.1±5.1 nm, and width 27.9±1.8 nm. The ZnO[b] NPs were small and rod-shaped, average size was 18.5±1.2 nm, and width 6.8±0.5 nm (Figure 1A, Table 3). The size of ZnO[a] NPs detected via dynamic light scattering was 90.8 nm, and that of ZnO[b] NPs 49.4 nm (Figure 1B, Table 3). Both ZnO NP types were detected to be larger in water, evidencing the agglomeration effect of the particles in water. ζ-Potentials of both ZnO NP types were determined, and significant differences were not observed (ZnO[a] NPs 14.8±11.3 mV, ZnO[b] NPs 15.3±9.33 mV).

Zinc ions released from ZnO NPs in culture medium

To explore zinc-ion levels released from the two types of ZnO NPs in extracellular fluid, we detected zinc concentrations in the culture medium at various concentrations (Figure 1C). We found that zinc-ion levels in the culture medium increased in a concentration-dependent manner. The highest zinc concentration was nearly 6 μg/mL at a concentration of 100 μg/mL for the ZnO[a] NPs; this result was slightly lower

than that of the ZnO[b] NPs (nearly 6.7 μg/mL). Moreover, zinc concentrations in the culture medium following treatment with the two types of ZnO NPs at concentrations of 25 μg/mL and 50 μg/mL were approximately 2 μg/mL (nearly 30.7 μM) and 4 μg/mL (nearly 61.4 μM), respectively.

Trans-retinoic acid-induced SHSY5Y-cell differentiation

We used trans-retinoic acid to differentiate SHSY5Y cells and observed cell-morphology changes at 0, 3, 6, 9, 12, and 15 days (Figure 2). We found that SHSY5Y cells were polygonal without any activation. After trans-retinoic acid incubation, cells extended a few pseudopodia, which were elongated in a time-dependent manner. Moreover, a large number of SHSY5Y cells exhibited spindle shapes after trans-retinoic acid treatment for more than 12 days.

Two types of ZnO NP-induced viability changes in SHSY5Y cells

We detected the viability of SHSY5Y cells after treatment with the two ZnO NP types and $ZnCl_2$. We did not observe toxic effects from the ZnO NPs after 2 hours of treatment. Following ZnO[a] NP treatment (Figure 3A), no significant viability changes were observed in SHSY5Y cells at concentrations ≤20 μg/mL for any time point. However, ZnO[a] NP concentrations >20 μg/mL showed potent viability decrease in a time-dependent manner. Following ZnO[b] NP treatment (Figure 3B), the results showed concentration-dependent toxic effects at 6, 12, and 24 hours. Toxic effects were more significant at concentrations ≥20 μg/mL.

When cells were treated with ZnO NPs at concentrations below 20 μg/mL, slight toxic effects were observed with the ZnO[b] NPs, while no toxic effects were detected with the ZnO[a] NPs. Moreover, compared with ZnO[a] NPs, with ZnO[b] NPs at concentrations ≥20 μg/mL, we detected more significant cell-viability decrease. ZnO[b] NPs decreased cell viability to <10% at the highest concentration (100 μg/mL) after 24 hours, while ZnO[b] NPs reduced cell viability to 20%.

Our results showed that $ZnCl_2$ had significantly higher toxic effects than the two ZnO NP types at the same zinc

A

ZnOᵃ NPs   ZnOᵇ NPs

B

C
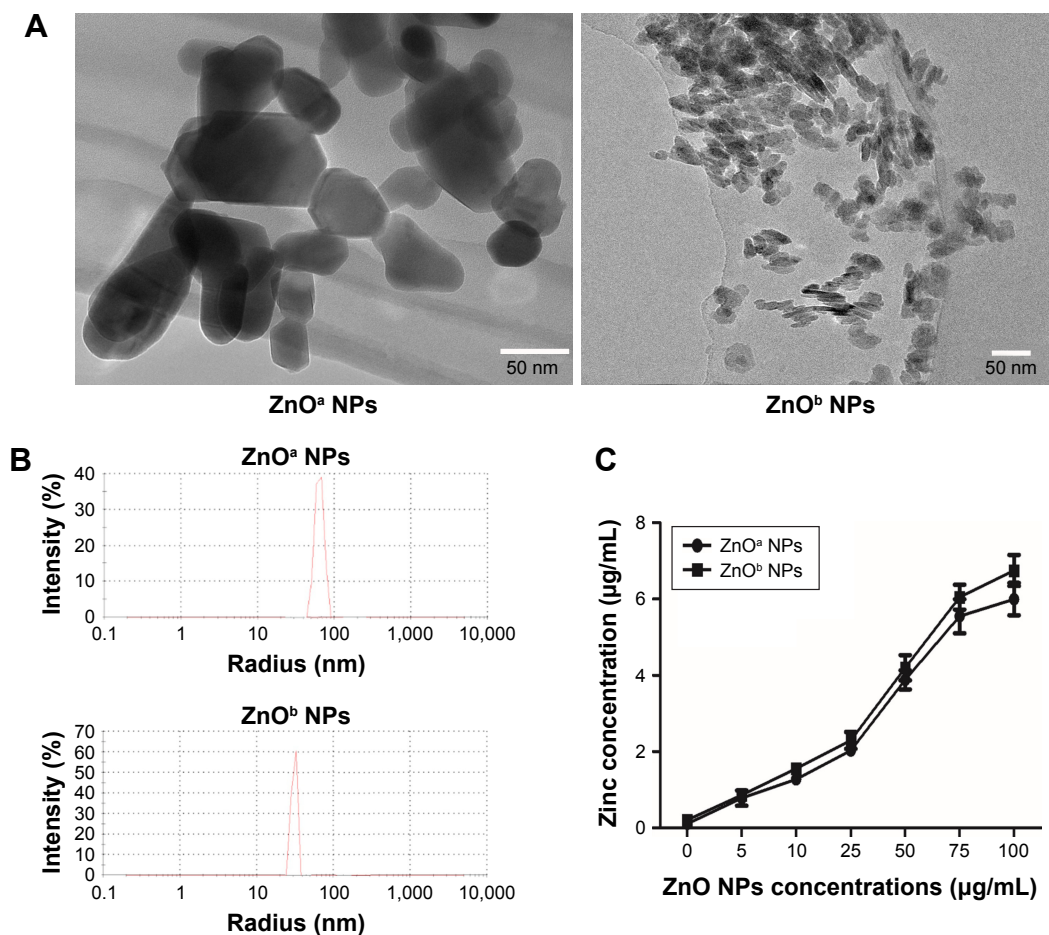
Figure 1 Characterization of ZnO NPs.
Notes: ZnO NP morphology and size were detected using TEM (**A**). DLS (**B**) was used to determine NP distribution in an aqueous solution. (**C**) Zinc concentrations in supernatants of ZnO NP suspensions at various concentrations (0, 5, 10, 25, 50, 75, and 100 µg/mL). Scale bar =50 nm.
Abbreviations: DLS, dynamic light scattering; NPs, nanoparticles; TEM, transmission electron microscopy.

molar concentration (Figure 3C). Similar toxic effects in a time- and concentration-dependent manner were observed. Following $ZnCl_2$ treatment, toxic effects were detected at concentrations of 61.4 µM, and cell viability rapidly decreased to approximately 10% at a concentration of 122.9 µM after 24 hours of treatment. Moreover, a significant decrease in cell viability was observed with $ZnCl_2$ treatment for 2 hours.

Immunocytochemistry of intracellular zinc ions and lysosomes

We detected the zinc ion-shedding process in cells using immunocytochemistry after exposure to ZnOᵃ NPs (Figure 4A)

Table 3 Characterization of ZnO NPs

Type of particle	Average size (nm)	Average width (nm)	DLS (nm)	ζ-Potential (mV)	Surface area (m²/g)
ZnOᵃ	47.1±5.1	27.9±1.8	90.8	14.8±11.3	32.17
ZnOᵇ	18.5±1.2	6.8±0.5	49.4	15.3±9.33	17.03

Abbreviations: DLS, dynamic light scattering; NPs, nanoparticles.

and ZnOᵇ NPs (Figure 4B). Our results showed that the two ZnO NP types released zinc ions in the intracellular region. Zinc ions were detected rapidly after 1 hour, and ZnOᵇ NPs produced a significantly higher level of zinc ions in the intracellular region after 1 hour than ZnOᵃ NPs. After the 3- and 5-hour treatments, significant zinc-fluorescence intensity was detected following exposure to both types of ZnO NPs. In this study, we also detected lysosomes, which are a type of organelle under acidic conditions. We found that regions with zinc ions merged with the lysosomes at all time points following exposure to both types of ZnO NPs.

NAC inhibition effects on ZnO NP-induced cytotoxicity

In this study, we detected inhibition effects of NAC, which is an ROS-scavenging agent. The results showed that NAC exhibited inhibition effects on ZnOᵃ NP- and ZnOᵇ NP-induced cell-viability loss after 24 hours of treatment (Figure 5A), particularly at concentrations ≥40 µg/mL. Following ZnOᵃ NP and ZnOᵇ NP treatments, cell viability decreased to nearly
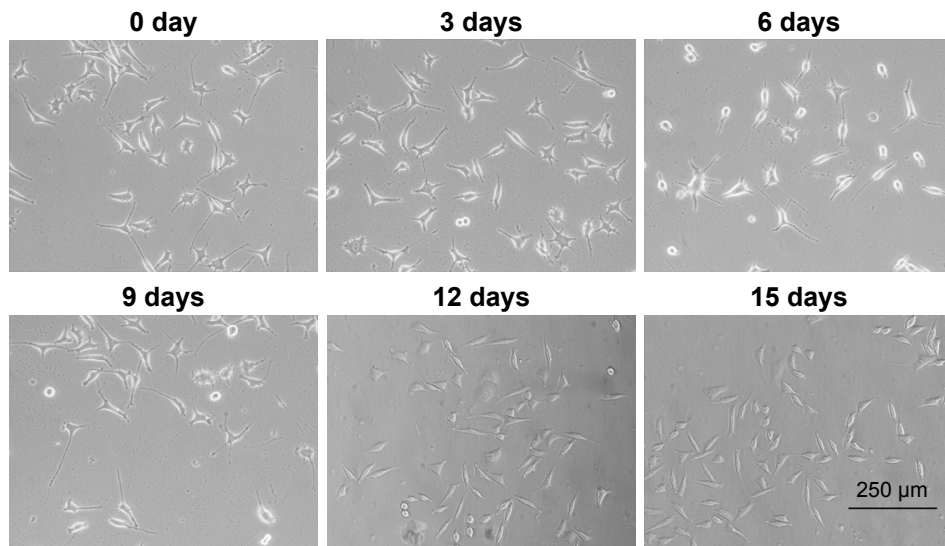
Figure 2 Trans-retinoic acid-induced SHSY5Y-cell differentiation. Scale bar =250 μm. Magnification ×200.
**Notes:** SHSY5Y cells were differentiated using trans-retinoic acid. Cell-morphology changes were observed at 0, 3, 6, 9, 12, and 15 days.
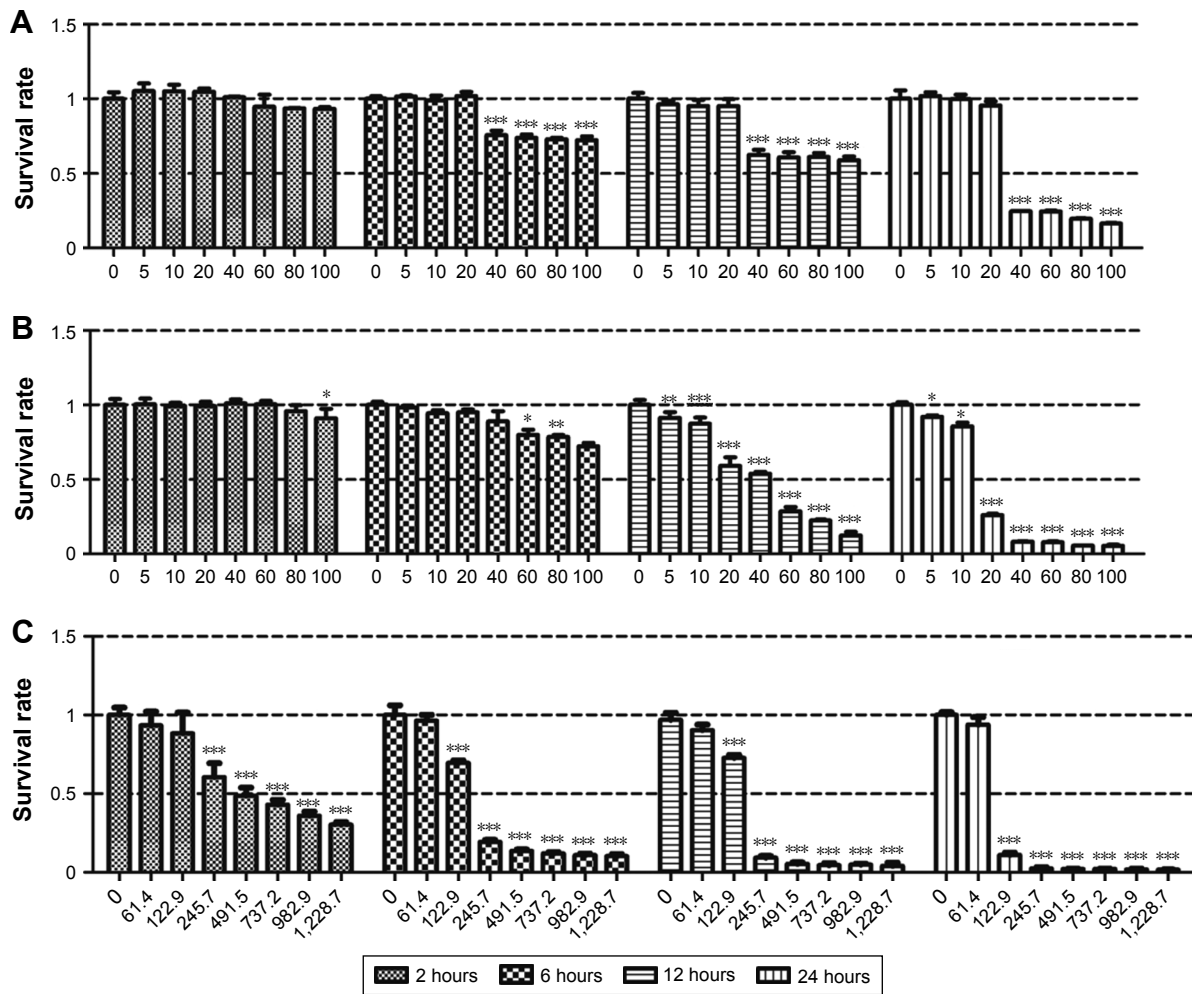
Figure 3 Two types of ZnO NP- and ZnCl₂-induced toxic effects in the SHSY5Y cells.
Notes: SHSY5Y cells were treated with ZnO NPs at concentrations of 0, 5, 10, 20, 40, 60, 80, and 100 μg/mL and ZnCl₂ at concentrations of 0, 61.4, 122.9, 245.7, 491.5, 737.2, 982.9, and 1,228.7 μM for 2, 6, 12, and 24 hours, and then cell viability was detected via CCK-8 assay. (**A**) ZnO[a] NP-induced SHSY5Y cell-viability changes. (**B**) ZnO[b] NP-induced SHSY5Y cell-viability changes. (**C**) ZnCl₂-induced SHSY5Y cell-viability changes. Results shown as means ± SEM. *$P<0.05$; **$P<0.01$; ***$P<0.001$.
Abbreviation: NPs, nanoparticles.
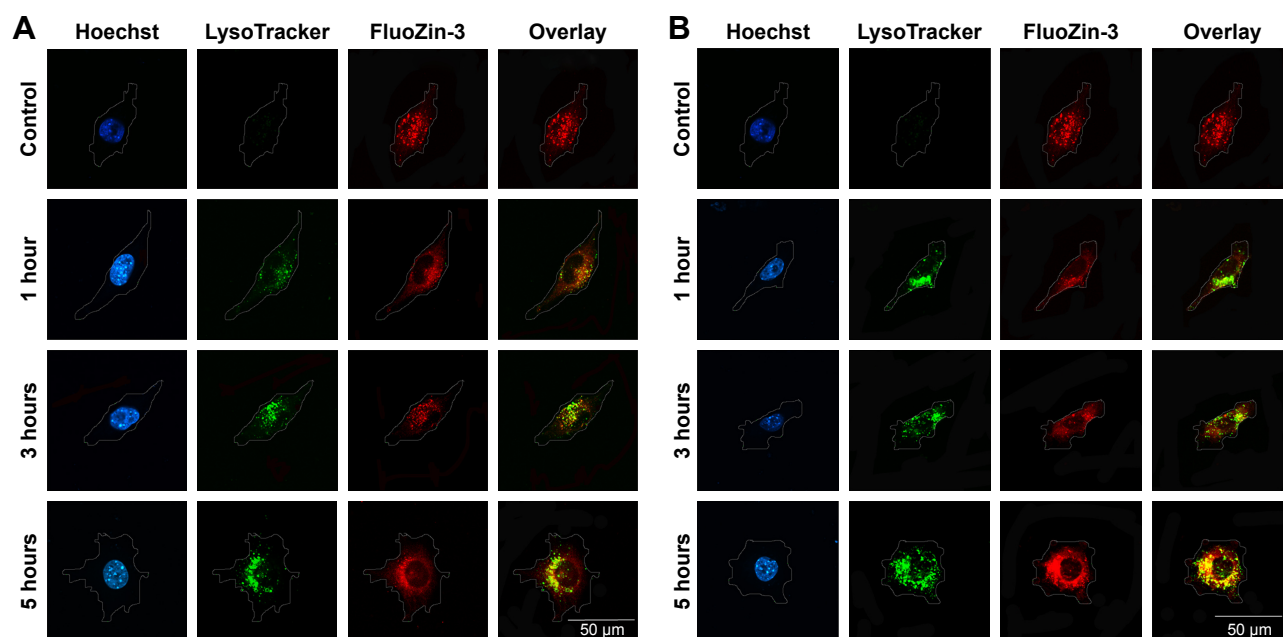
Figure 4 Confocal microscopy investigation of cellular distribution of lysosomes and zinc ions in SHSY5Y cells after the two ZnO NP treatments.
Notes: After SHSY5Y cells had been treated with ZnO[a] NPs (**A**) and ZnO[b] NPs (**B**) at a concentration of 50 μg/mL for 1, 3, and 5 hours, the cells were loaded with FluoZin-3 (green), LysoTracker (red), and Hoechst 33342 (blue). We observed almost no zinc-ion fluorescence in the control group, but significant zinc ions (green) were observed within 1 hour after ZnO NP treatment and a slight increase in the zinc fluorescence (green) was observed in a time-dependent manner. Treatment with ZnO[b] NPs exhibited higher fluorescence values than treatment with ZnO[a] NPs at 1 hour. Moreover, significant overlaps (yellow) between the cellular zinc ions and lysosomes were observed at all time points. Scale bar =50 μm. Magnification ×600.
Abbreviation: NP, nanoparticle.

25% and 8%, respectively, at a concentration of 40 μg/mL; however, after NAC treatment, viability remained at nearly 100% and 92%, respectively. In addition, the inhibition effects of NAC weakened at concentrations ≥40 μg/mL. Cell viability of ZnO[a] NP- and ZnO[b] NP-treated cells in the presence of NAC was nearly 50% and 65%, respectively, at a concentration of 100 μg/mL. Moreover, we found that NAC also showed inhibition effects for $ZnCl_2$ after 24 h of treatment, particularly at concentrations of 122.9 μM and 245.7 μM (Figure 5A). Cell viability decreased to <10% after $ZnCl_2$ treatment at concentrations ≥491.5 μM, even when combined with NAC.

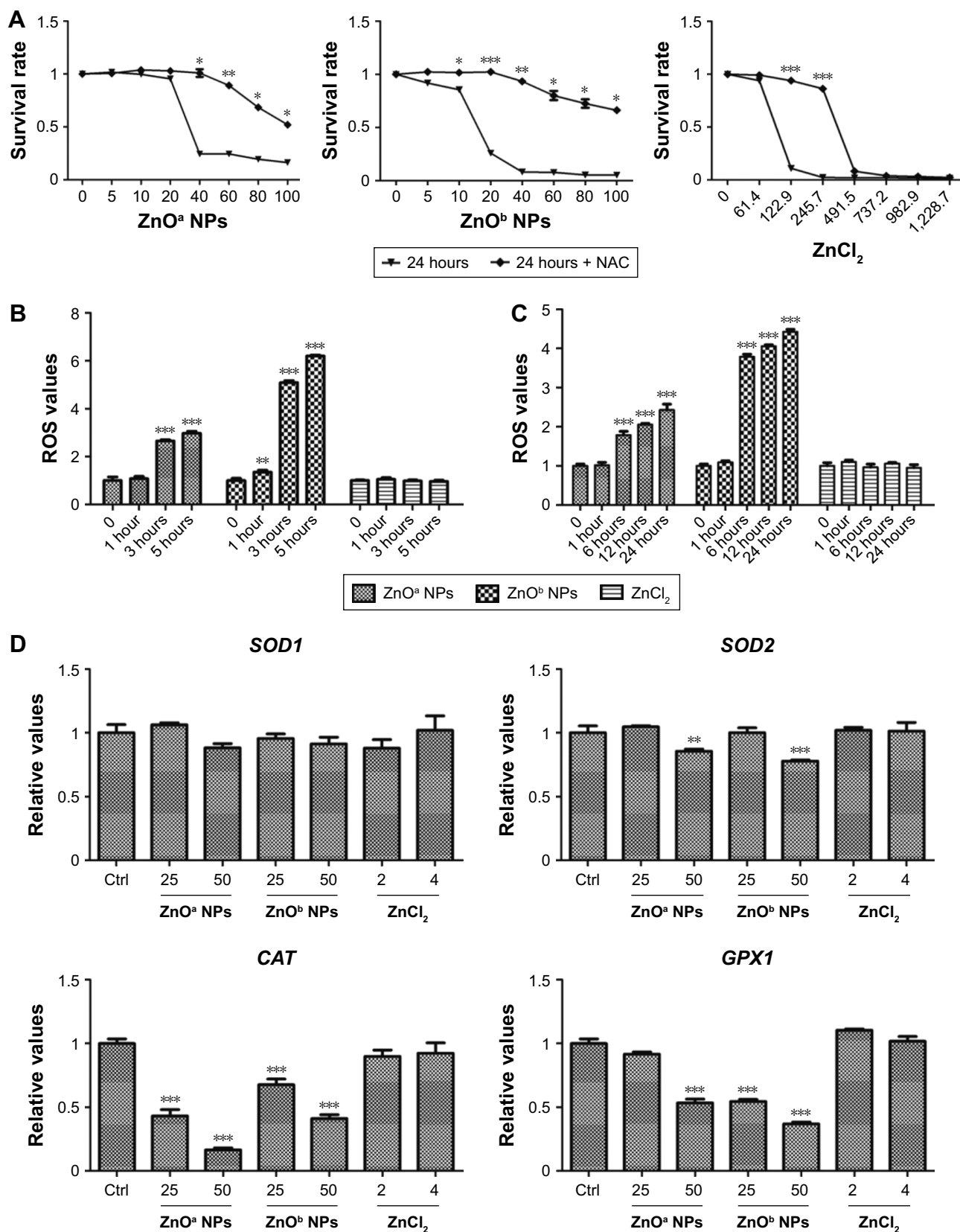## ZnO NP-induced ROS generation and oxidative stress-related gene changes

In this study, we detected ROS generation after ZnO NP exposure to SHSY5Y cells (Figure 5B). Our results showed that the two types of ZnO NPs induced ROS generation in SHSY5Y cells, and this effect was most significant after 3 and 5 hours, respectively, at a concentration of 50 μg/mL. ZnO[b] NPs showed higher ROS generation than ZnO[a] NPs. Moreover, significant ROS generation was observed after 1 hour following ZnO[b] NP exposure, but not following ZnO[a] NPs exposure. Meanwhile, we also detected ROS generation after zinc-ion treatment at a concentration

of 4 μg/mL (Figure 5B), which was similar to the zinc concentrations in the supernatants of these two ZnO NP types (50 μg/mL).

ROS generation was also detected after ZnO NP exposure at a concentration of 25 μg/mL (Figure 5C). Significant ROS generation was detected after 6, 12, and 24 hours of treatment with the two types of ZnO NPs, while significant ROS changes were not observed after 1 hour of treatment. ZnO[b] NPs showed higher ROS generation than ZnO[a] NPs after long-term treatment. The zinc ions did not show potent ROS generation at a concentration of 2 μg/mL, which was similar to the zinc concentrations in the supernatants of the two types of ZnO NPs (25 μg/mL).

We then detected the changes in oxidative stress-related gene expression after 1-hour treatment with ZnO NPs and zinc ions (Figure 5D). Significant oxidative stress-related gene changes were observed after treatment with the two ZnO NPs types in a concentration-dependent manner. A potent decrease in gene-expression levels was detected at 50 μg/mL, including such genes as *SOD2*, *CAT*, and *GPX1*. However, ZnO NPs induced a decrease in expression levels of the *GPX1* and *CAT* genes at 25 μg/mL. In addition, zinc ions, regardless of whether the concentration was 2 μg/mL or 4 μg/mL, did not induce significant changes in gene levels.

Figure 5 NAC inhibition effects on ZnO NP-induced cytotoxicity, ZnO NP-induced ROS generation, and oxidative stress-related gene changes.
Notes: (**A**) SHSY5Y cells were treated with ZnOª NPs, ZnOᵇ NPs, and ZnCl₂ at various concentrations for 24 hours, and NAC (10 mM) was incubated simultaneously. Cell-viability data were obtained using CCK-8 assay. (**B**) ROS values in SHSY5Y cells after the ZnO NPs (50 μg/mL) and ZnCl₂ (4 μg/mL) treatments for 1, 3 and 5 hours. (**C**) ROS values in SHSY5Y cells after the ZnO NPs (25 μg/mL) and ZnCl₂ (2 μg/mL) treatments for 1, 6, 12 and 24 hours. (**D**) Oxidative stress-related gene changes in SHSY5Y cells after treatment with ZnO NPs and ZnCl₂. Results shown as means ± SEM of three independent experiments. *$P<0.05$; **$P<0.01$; ***$P<0.001$.
Abbreviations: NAC, *N*-acetylcysteine; NP, nanoparticle; ROS, reactive oxygen species.

ZnO NP-induced apoptosis in SHSY5Y cell line

Apoptosis levels in SHSY5Y cells were detected after ZnO NP exposure at various concentrations (Figure 6A). The results indicated that ZnO NPs induced apoptosis in a concentration-dependent manner. Following ZnO^a NP exposure for 5 hours, late-apoptosis levels were 2.3%, 3.1%, and 3.1% at concentrations of 20, 40, and 60 μg/mL, respectively. Late-apoptosis levels were 2.6%, 4.6%, and 6.2% at the same concentrations of ZnO^b NP exposure, respectively. We found that the two ZnO NP types induced apoptosis in SHSY5Y cells, but ZnO^b NPs induced higher apoptosis levels than ZnO^a NPs. Moreover, we detected apoptosis levels in the presence of zinc ions. Late-apoptosis levels were 0.5%, 1.2%, and 1.1% for zinc ions at concentrations of 1.6, 3.2, and 4.8 μg/mL, respectively, which were similar to zinc concentrations in the ZnO supernatants: 20, 40, and 60 μg/mL. Moreover, we found that zinc ions at a concentration of 10 μg/mL induced significant apoptosis changes (late-apoptosis levels 33.8%) and near-complete cell death (99.9%) at a concentration of 20 μg/mL.

Apoptosis-related genes were detected in this study after treatment with ZnO NPs and zinc ions for 1 hour (Figure 6B), and the expression of three apoptosis-related genes increased after ZnO NP treatment. For *BAX*, a proapoptotic gene, a nearly sixfold increase was observed after treatment with ZnO NPs at a concentration of 50 μg/mL, and compared to the control group, ZnO^b NPs (25 μg/mL) induced a nearly fourfold change in *BAX* expression; this value was higher than that of the ZnO^a NPs at a similar concentration (nearly double). We also detected a slight increase in the *BCL2* gene levels after treatment with the two ZnO NP types in a concentration-dependent manner. Furthermore, the *BAX:BCL2* ratio increased significantly, indicating proapoptotic effects. ZnO^a NPs induced higher changes in gene-expression levels than ZnO^b NPs at a concentration of 50 μg/mL. For *CYTC*, a potent increase in gene-expression levels was observed for the two ZnO NP types at various concentrations. Zinc ions did not induce any gene changes at a concentration of 2 μg/mL. However, a slight increase in gene-expression levels of *BAX* and *BCL2* was observed after zinc-ion treatment at a concentration of 4 μg/mL.

ZnO NP-induced cytoskeleton changes in SHSY5Y cell line

Morphology changes in SHSY5Y cells after exposure to ZnO^a NPs (Figure 7A) and ZnO^b NPs (Figure 7B) were observed. We used confocal microscopy to examine actin filaments and the microtubule system, and found that actin filaments were distributed in the cell membrane, while microtubules were located in the intracellular region between the cell nucleus and cell membrane. Moreover, there were no significant morphological changes in SHSY5Y cells after the two types of ZnO NP treatments. However, following ZnO^b NP treatment, actin agglomeration was observable after 3 hours, and particularly after 5 hours. Moreover, the microtubule system was observed to be encompassed by the cell nucleus, and the region between the cell membrane and cell nucleus was dull compared with that in the control group.

Discussion

ZnO nanomaterials are the most widely applied nanomaterials worldwide, and they are considered important components of cosmetics and electronic equipment. In this study, we explored the toxicological effects of ZnO NPs using two types of ZnO NPs with various sizes. Many studies have indicated that the physicochemical properties of nanomaterials, including size,[15,25–27] shape,[28–30] surface area,[31] ζ-potential,[27,32] and composition, greatly affect their toxicological effects.[23] The results of our study indicated that the ZnO^a NPs and ZnO^b NPs were rod-shaped with a low aspect ratio. Previous studies have shown that high-aspect-ratio particles, such as nanotubes, nanowires, and nanorods, might have more significant toxic effects.[28–30] However, in this study, we believe that shape was not the main factor in toxicity discrepancy when comparing these two nanomaterials with low-aspect-ratio particles. Müller et al[33] attributed the toxic effects of ZnO nanowires to released zinc ions, rather than to the high aspect ratio, implying that the rapid dissolution of ZnO may have reduced the effect of the NP shape. The average size of the ZnO^a NPs was 47.1±5.1 nm, with width 27.9±1.8 nm, and the average size of the ZnO^b NPs was 18.5±1.2 nm, with width 6.8±0.5 nm, which was smaller than that of the ZnO^a NPs. As is well known, NPs can form agglomerates easily.[34] Our results indicated that these two particle types showed agglomeration in the correct solvent, and the average sizes of the ZnO^a NPs and ZnO^b NPs in solvent were 90.8 nm and 49.4 nm. ZnO^a NPs were larger in solvent than ZnO^b NPs.

SHSY5Y cells are the most frequently used cell models and are derived from neuroblastoma. The differentiation of SHSY5Y cells is often induced by trans-retinoic acid to investigate their more neuron-like properties, such as their morphological changes and neuronal phenotypes.[35] Undifferentiated SHSY5Y cells have also been used as cell models in studies in the field of neuroscience.[36–38] However, a previous study has indicated that the undifferentiated SKNSH
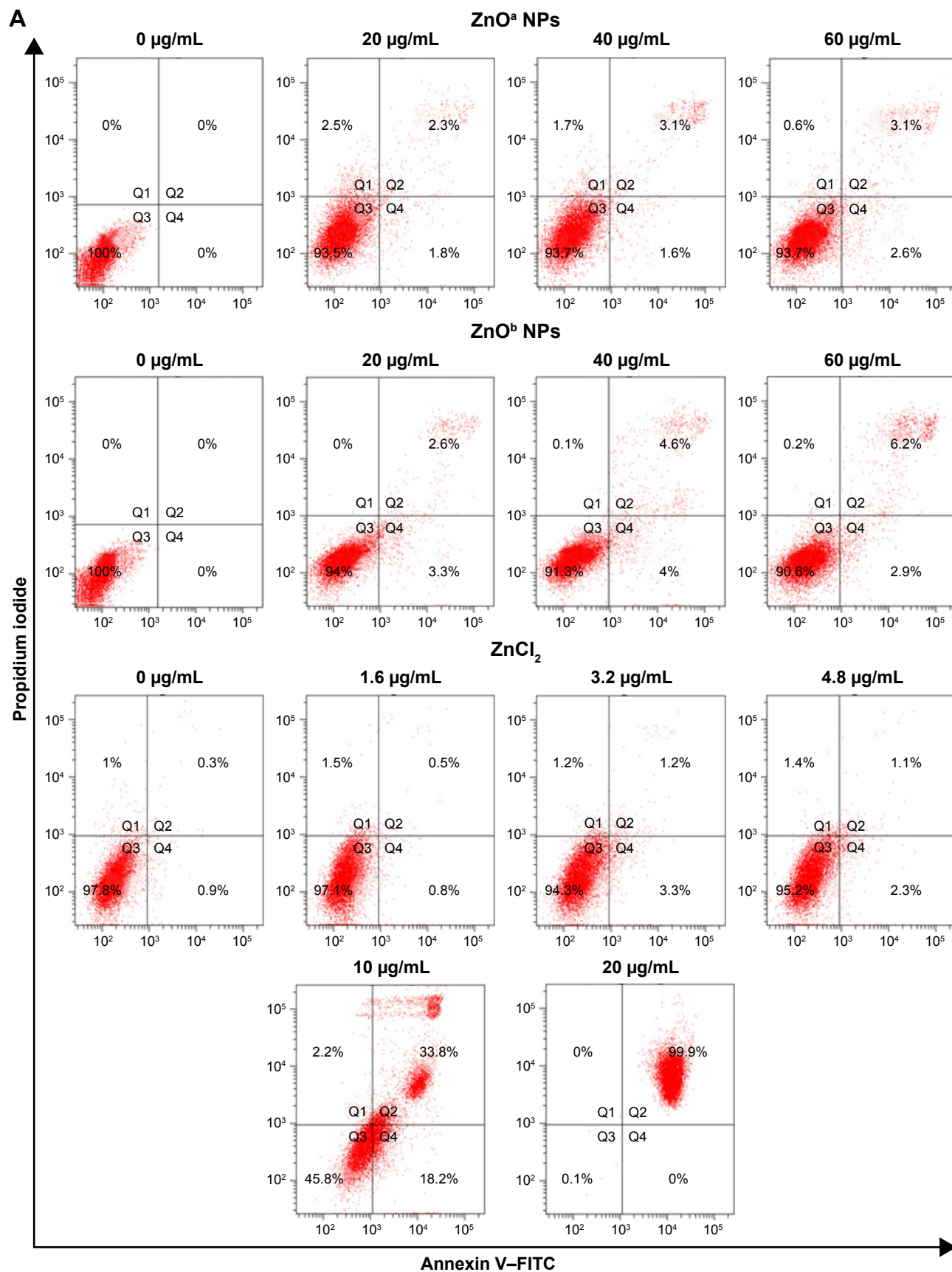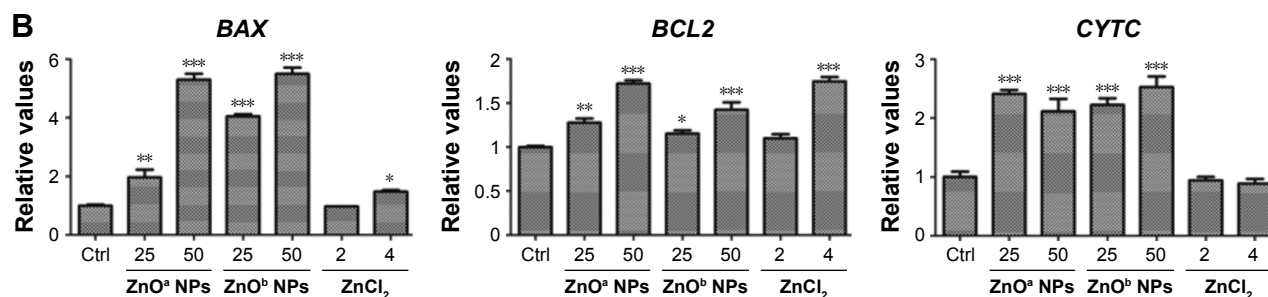
A

Figure 6 (*Continued*)

B

Figure 6 Two types of ZnO NP-induced apoptosis in SHSY5Y cells.
Notes: (**A**) After SHSY5Y cells had been treated with ZnO[a] NPs, ZnO[b] NPs, and ZnCl$_2$ at various concentrations for 5 hours, cell-apoptosis levels were detected. (**B**) Apoptosis-related changes in gene expression in SHSY5Y cells after treatment with ZnO NPs and ZnCl$_2$. Results shown as means ± SEM of three independent experiments. *$P < 0.05$; **$P < 0.01$; ***$P < 0.001$.
**Abbreviations:** FITC, fluorescein isothiocyanate; NP, nanoparticle.

cell line, which was the original cell line of SHSY5Y cells, did not show significant neuronal properties compared with those of trans-retinoic acid-differentiated SKNSH cells.[39] In our study, trans-retinoic acid-differentiated SHSY5Y cells exhibited significant morphological changes that were more consistent with those of the neurophenotypes. We found that neurites were extended and some cells became spindle-shaped within 3 days. After 12 days of activation, almost all cells had a spindle shape.

Our results showed that ZnO NPs had significant toxic effects on the SHSY5Y cell line. Cell viability decreased rapidly when ZnO NP concentrations were >40 µg/mL, and there were no toxic effects after short-term exposure (2 hours). Cell viability decreased to <50% after 24 hours' exposure at concentrations ≥40 µg/mL. Many studies have shown that the cytotoxicity of nanomaterials depends on their size.[15,25–27] Our study showed similar results. Compared to ZnO[a] NP treatment, we found a larger number of significant

toxic effects following ZnO[b] NP treatment. ZnO[b] NPs showed significant toxic effects, which decreased cell viability to almost 25% after 24 hours' exposure at a concentration of 20 µg/mL; however, there were no toxic effects following ZnO[a] NP treatment at the same concentration.

James et al[40] found that ZnO NPs (20 µg/mL) induced a fourfold intracellular zinc-level increase, while ZnCl$_2$ induced only a 1.3-fold increase (15 µg/mL). These authors demonstrated that zinc ions were the main factor in ZnO NP-induced cytotoxicity. Another study showed that ZnCl$_2$ induced toxic effects that were similar to those induced by ZnO NPs, and the oxidative stress and interactions of the zinc ions and their cellular targets were the main factors in ZnO NP-induced toxic response.[25] Moreover, ZnO NP-induced toxic response decreased after treatment with EDTA, CaCl$_2$,[41] or iron doping.[42,43] These materials/methods can bind zinc ions or decrease ZnO NP solubility. As our results indicated, zinc ions were more toxic than ZnO NPs
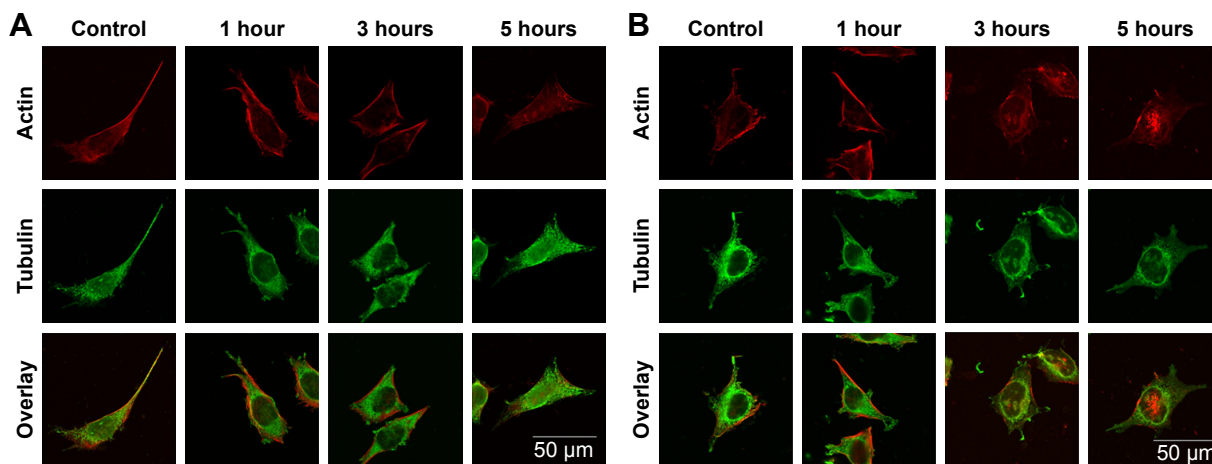
Figure 7 Two types of ZnO NP-induced cytoskeleton changes.
Notes: After SHSY5Y cells had been treated with ZnO[a] NPs (**A**) and ZnO[b] NPs (**B**) at concentrations of 50 µg/mL for 1, 3, and 5 hours, cytoskeleton changes were assessed based on alterations in actin (red) and tubulin systems (green). Scale bar =50 µm. Magnification ×600.
Abbreviation: NP, nanoparticle.

at the same zinc molar concentration. We detected zinc-ion concentrations in the supernatants after treatment with the two ZnO NP types, and our results showed that zinc-ion levels in the supernatants were low, much less than total zinc content in the ZnO NPs. Meanwhile, the zinc-ion level in the supernatants was approximately 4 µg/mL (approximately 61.4 µM) following treatment with the two ZnO NP types at a concentration of 50 µg/mL, which did not induce any toxic effects in the SHSY5Y cells. We propose that the zinc ions in the supernatants were not the main factor in the ZnO NP-induced toxicological profile.

As a type of ion-shedding particle, ZnO NPs show high solubility in acidic environments.[9] Wang et al[44] found that vitamin C enhanced ZnO NP-induced toxicity due to its acidity, thereby accelerating ZnO NP dissolution. Other studies have indicated that ZnO NPs can dissolve in lysosomes in an acidic environment.[45,46] We found ZnO NP dissolution in the intracellular acid of vesicular organelles within 1 hour and that ZnO[b] showed a higher ion-shedding ability than ZnO[a]. We believe that the zinc ion-shedding process can occur in the intracellular region and release zinc ions persistently, and this behavior is likely the main factor related to ZnO NP-induced toxic effects. We suggest that the zinc ions derived from the ZnO NPs played a major role in the related toxic responses, in which the ZnO NPs released zinc ions and induced cytotoxicity persistently. This persistent ion-shedding process may explain why the ZnO NPs induced a much weaker toxic response than ZnCl$_2$ at the same molar concentration of zinc.

Some studies have indicated that ZnO NPs can alter the expression of oxidative- and apoptosis-related genes and proteins.[14,47] As is well known, oxidative stress is considered a key factor in nanomaterial-induced toxic effects that trigger autophagy and apoptosis through distinct mechanisms.[41,48–51] Oxidative stress is produced via ROS generation and a decrease in antioxidant factors, such as superoxide dismutase and glutathione, which have been reported to be the main factors in ZnO NP-induced toxic responses.[52–54] Kim et al[55] indicated that ROS, mainly O^{2-}, were likely the main factors involved in ZnO NP-induced cell death, and the amount of ROS generated after ZnO NPs penetrate cells has been determined in macrophages.[3] Our results supported this hypothesis. We found that NAC incubation significantly inhibited ZnO NP-induced decrease in cell viability. In addition, significant ROS generation and inhibition effects on the expression of antioxidant genes, particularly *CAT* and *GPX1*, were observed after treatment with the two types of ZnO NPs. Cells treated with ZnO[b] NPs produced higher ROS levels than with ZnO[a] NPs, implying that the ROS generation depended on the

particle size. Li et al[31] found that smaller particles produced more ROS and exhibited higher toxic effects due to their larger surface area, allowing them to absorb more photons. Further, ZnO NP-induced oxidative stresses are likely due to their released zinc ions, which can activate ROS generation.[56] According to our study, NAC significantly inhibited zinc ion-induced toxic effects, implying that ROS indeed play a crucial role in zinc ion-induced toxic effects. In addition, zinc ions released in the culture medium did not induce ROS generation or antioxidant-related gene changes. We think the persistent zinc ions release that occurred in the intracellular acidic vesicular organelles was probably the main cause of intracellular ROS generation.

We observed significant apoptosis after short-term ZnO NP exposure, and treatment with ZnO[b] NPs resulted in higher apoptosis levels than treatment with ZnO[a] NPs. The zinc ions in the supernatants were probably not the main factor in apoptosis, while zinc ions at high concentrations significantly induced cell apoptosis, resulting in death. We think the persistent zinc ion release in the intracellular regions was probably the key factor in ZnO-induced apoptosis. Mitochondria can sequester zinc ions into intracellular regions, leading to zinc-ion concentration elevation in the mitochondria and mitochondria dysfunction, and ultimately initiating apoptotic pathways, including the Bcl2-apoptosis pathway.[57,58] Our results showed that apoptosis pathways were initiated after treatment with the two types ZnO NPs, particularly for the Bcl2 apoptotic family. Moreover, ZnO NP-induced ROS generation was regarded as one of the main causes of the initiation of apoptosis-related pathways.[4]

The SHSY5Y cell line is a traditional model in neuroscience. The cytoskeleton metabolism is a dynamic biological process that exhibits characteristics between polymerization and depolymerization; this process promotes and sustains cell morphology and functions. Many studies have indicated that nanomaterial exposure induces cytoskeleton disruption and cell-morphology changes.[59–62] In our study, we did not observe significant cell-morphology changes in SHSY5Y cells, but some actin clustering was observed after ZnO NP treatments of >3 hours, indicating that dynamic actin polymerization was disrupted. Xu et al[59] found that Ag NP exposure induced structural cell-cytoskeleton changes by altering the actin and tubulin systems. Chen et al[63] observed cell shrinkage and actin rearrangement after Al NP treatment. Studies have attributed NP-induced cell-cytoskeleton changes to ROS generation.[64,65] We suggest that these actin disturbances were likely attributable to ZnO NP-induced zinc-ion release and ROS generation.
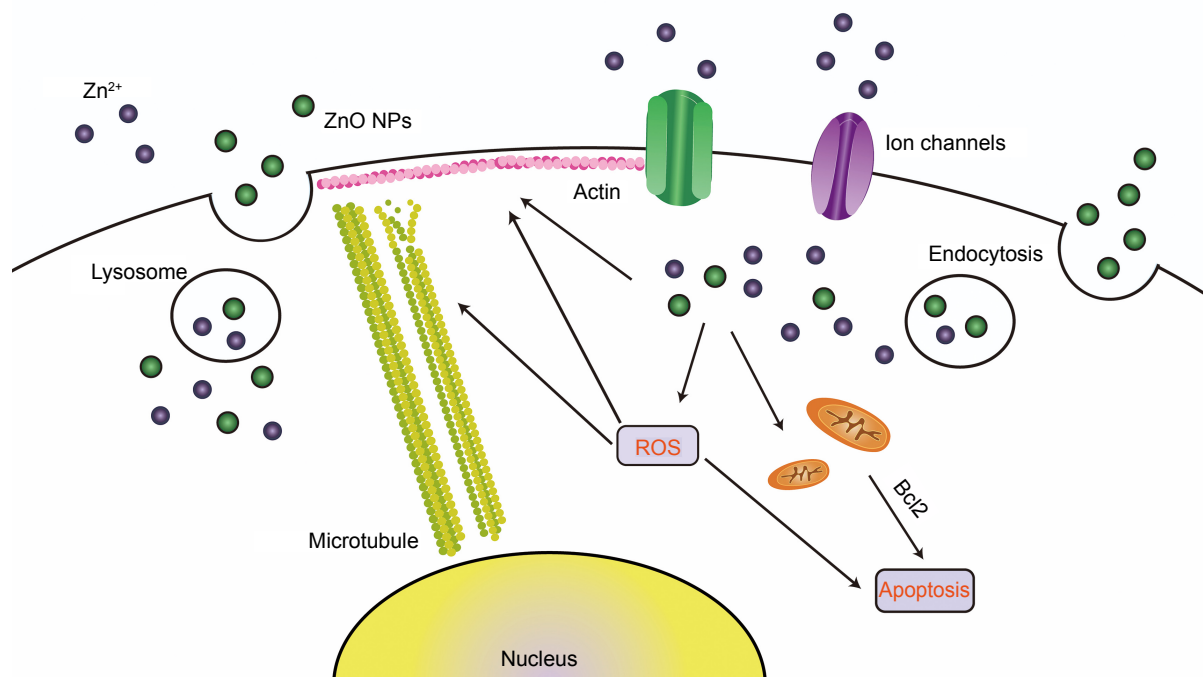
Figure 8 ZnO NP-induced toxic effects in SHSY5Y cells.
Notes: ZnO NPs released zinc ions into the culture medium. Undissolved particles were endocytosed and dissolved into lysosomes due to the acidic environment. ZnO NPs and zinc ions induce ROS generation, resulting in apoptosis and cytoskeleton disruption.
Abbreviations: NP, nanoparticle; ROS, reactive oxygen species.

Conclusion

In conclusion, our data indicated that ZnO NPs induced significant cytotoxicity in a size-dependent manner, and detailed information is provided in Figure 8. ROS generation was observed after ZnO NP treatment, and was a main factor in ZnO NP-induced toxic effects, which included decreasing cell viability and apoptosis. The ZnO NPs dissolved in acidic vesicular organelles and released zinc ion, which likely played a crucial role in the related toxic responses. The cytoskeleton changes were one of the main toxic effects of ZnO NPs. The findings of this study provide deep insights into the effects of NPs of different sizes, particularly soluble NPs, such as ZnO, and provide more useful toxicological information on nanomaterials.

Acknowledgments

Disclosure

The authors report no conflicts of interest in this work.

References

1. Nowack B, Bucheli TD. Occurrence, behavior and effects of nanoparticles in the environment. *Environ Pollut*. 2007;150(1):5–22.
2. Giovanni M, Yue J, Zhang L, Xie J, Ong CN, Leong DT. Pro-inflammatory responses of RAW264.7 macrophages when treated with ultralow concentrations of silver, titanium dioxide, and zinc oxide nanoparticles. *J Hazard Mater*. 2015;297:146–152.
3. Song W, Zhang J, Guo J, et al. Role of the dissolved zinc ion and reactive oxygen species in cytotoxicity of ZnO nanoparticles. *Toxicol Lett*. 2010;199(3):389–397.
4. Setyawati MI, Tay CY, Leong DT. Effect of zinc oxide nanomaterials-induced oxidative stress on the p53 pathway. *Biomaterials*. 2013;34(38):10133–10142.
5. Liu J, Feng X, Wei L, Chen L, Song B, Shao L. The toxicology of ion-shedding zinc oxide nanoparticles. *Crit Rev Toxicol*. 2016;46(4):348–384.
6. Cho WS, Kang BC, Lee JK, Jeong J, Che JH, Seok SH. Comparative absorption, distribution, and excretion of titanium dioxide and zinc oxide nanoparticles after repeated oral administration. *Part Fibre Toxicol*. 2013;10:9.
7. Palomäki J, Karisola P, Pylkkänen L, Savolainen K, Alenius H. Engineered nanomaterials cause cytotoxicity and activation on mouse antigen presenting cells. *Toxicology*. 2010;267(1–3):125–131.
8. Watson C, Ge J, Cohen J, Pyrgiotakis G, Engelward BP, Demokritou P. High-throughput screening platform for engineered nanoparticle-mediated genotoxicity using CometChip technology. *ACS Nano*. 2014;8(3):2118–2133.
9. Donaldson K, Schinwald A, Murphy F, et al. The biologically effective dose in inhalation nanotoxicology. *Acc Chem Res*. 2013;46(3):723–732.
10. Jiang C, Hsu-Kim H. Direct in situ measurement of dissolved zinc in the presence of zinc oxide nanoparticles using anodic stripping voltammetry. *Environ Sci Process Impacts*. 2014;16(11):2536–2544.

11. Comfort KK, Braydich-Stolle LK, Maurer EI, Hussain SM. Less is more: long-term in vitro exposure to low levels of silver nanoparticles provides new insights for nanomaterial evaluation. *ACS Nano*. 2014;8(4): 3260–3271.

12. Jiang X, Miclaus T, Wang L, et al. Fast intracellular dissolution and persistent cellular uptake of silver nanoparticles in CHO-K1 cells: implication for cytotoxicity. *Nanotoxicology*. 2015;9(2):181–189.

13. Zhao J, Xu L, Zhang T, Ren G, Yang Z. Influences of nanoparticle zinc oxide on acutely isolated rat hippocampal CA3 pyramidal neurons. *Neurotoxicology*. 2009;30(2):220–230.

14. Valdiglesias V, Costa C, Kiliç G, et al. Neuronal cytotoxicity and genotoxicity induced by zinc oxide nanoparticles. *Environ Int*. 2013;55: 92–100.

15. Sahu D, Kannan GM, Vijayaraghavan R. Size-dependent effect of zinc oxide on toxicity and inflammatory potential of human monocytes. *J Toxicol Environ Health A*. 2014;77(4):177–191.

16. Amara S, Slama IB, Omri K, et al. Effects of nanoparticle zinc oxide on emotional behavior and trace element homeostasis in rat brain. *Toxicol Industrial Health*. 2013;31(12):1202–1209.

17. Shrivastava R, Raza S, Yadav A, Kushwaha P, Flora SJ. Effects of sub-acute exposure to TiO₂, ZnO and Al₂O₃ nanoparticles on oxidative stress and histological changes in mouse liver and brain. *Drug Chem Toxicol*. 2014;37(3):336–347.

18. Yeh TK, Chen JK, Lin CH, et al. Kinetics and tissue distribution of neutron-activated zinc oxide nanoparticles and zinc nitrate in mice: effects of size and particulate nature. *Nanotechnology*. 2012;23(8):085102.

19. Kao YY, Cheng TJ, Yang DM, Wang CT, Chiung YM, Liu PS. Demonstration of an olfactory bulb-brain translocation pathway for ZnO nanoparticles in rodent cells in vitro and in vivo. *J Mol Neurosci*. 2012;48(2): 464–471.

20. Hsiao IL, Huang YJ. Effects of various physicochemical characteristics on the toxicities of ZnO and TiO nanoparticles toward human lung epithelial cells. *Sci Total Environ*. 2011;409(7):1219–1228.

21. Hanley C, Thurber A, Hanna C, Punnoose A, Zhang J, Wingett DG. The Influences of cell type and ZnO nanoparticle size on immune cell cytotoxicity and cytokine induction. *Nanoscale Res Lett*. 2009;4(12): 1409–1420.

22. Heng BC, Zhao X, Tan EC, et al. Evaluation of the cytotoxic and inflammatory potential of differentially shaped zinc oxide nanoparticles. *Arch Toxicol*. 2011;85(12):1517–1528.

23. Wang XZ, Yang Y, Li R, et al. Principal component and causal analysis of structural and acute in vitro toxicity data for nanoparticles. *Nanotoxicology*. 2014;8(5):465–476.

24. Deng X, Luan Q, Chen W, et al. Nanosized zinc oxide particles induce neural stem cell apoptosis. *Nanotechnology*. 2009;20(11):115101.

25. Feltis BN, Okeefe SJ, Harford AJ, Piva TJ, Turney TW, Wright PF. Independent cytotoxic and inflammatory responses to zinc oxide nanoparticles in human monocytes and macrophages. *Nanotoxicology*. 2012;6(7):757–765.

26. Prach M, Stone V, Proudfoot L. Zinc oxide nanoparticles and monocytes: impact of size, charge and solubility on activation status. *Toxicol Appl Pharmacol*. 2013;266(1):19–26.

27. Pan CH, Liu WT, Bien MY, et al. Effects of size and surface of zinc oxide and aluminum-doped zinc oxide nanoparticles on cell viability inferred by proteomic analyses. *Int J Nanomedicine*. 2014;9:3631–3643.

28. Bhattacharya D, Santra CR, Ghosh AN, Karmakar P. Differential toxicity of rod and spherical zinc oxide nanoparticles on human peripheral blood mononuclear cells. *J Biomed Nanotechnol*. 2014;10(4):707–716.

29. Ken D, Fiona AM, Rodger D, Craig AP. Asbestos, carbon nanotubes and the pleural mesothelium: a review of the hypothesis regarding the role of long fibre retention in the parietal pleura, inflammation and mesothelioma. *Particle and Fibre Toxicology*. 2010;7:5.

30. Schinwald A, Murphy FA, Jones A, Macnee W, Donaldson K. Graphene-based nanoplatelets: a new risk to the respiratory system as a consequence of their unusual aerodynamic properties. *ACS Nano*. 2012; 6(1):736–746.

31. Li Y, Zhang W, Niu J, Chen Y. Mechanism of photogenerated reactive oxygen species and correlation with the antibacterial properties of engineered metal-oxide nanoparticles. *ACS Nano*. 2012;6(6):5164–5173.

32. Zhang J, Dong G, Thurber A, et al. Tuning the properties of ZnO, hematite, and Ag nanoparticles by adjusting the surface charge. *Adv Mater*. 2012;24(9):1232–1237.

33. Müller KH, Kulkarni J, Motskin M, et al. pH-dependent toxicity of high aspect ratio ZnO nanowires in macrophages due to intracellular dissolution. *ACS Nano*. 2010;4(11):6767–6779.

34. Tso CP, Zhung CM, Shih YH, Tseng YM, Wu SC, Doong RA. Stability of metal oxide nanoparticles in aqueous solutions. *Water Sci Technol*. 2010;61(1):127–133.

35. Pahlman S, Ruusala AI, Abrahamsson L, Mattsson ME, Esscher T. Retinoic acid-induced differentiation of cultured human neuroblastoma cells: a comparison with phorbolester-induced differentiation. *Cell Differ*. 1984;14(2):135–144.

36. Levites Y, Youdim MB, Maor G, Mandel S. Attenuation of 6-hydroxy-dopamine (6-OHDA)-induced nuclear factor-κB (NF-κB) activation and cell death by tea extracts in neuronal cultures. *Biochem Pharmacol*. 2002;63(1):21–29.

37. Lee JH, Shin SY, Kim S, Choo J, Lee YH. Suppression of PTEN expression during aggregation with retinoic acid in P19 mouse embryonal carcinoma cells. *Biochem Biophys Res Commun*. 2006;347(3):715–722.

38. Xue S, Jia L, Jia J. Hypoxia and reoxygenation increased BACE1 mRNA and protein levels in human neuroblastoma SH-SY5Y cells. *Neurosci Lett*. 2006;405(3):231–235.

39. Lombet A, Zujovic V, Kandouz M, et al. Resistance to induced apoptosis in the human neuroblastoma cell line SK-N-SH in relation to neuronal differentiation: role of Bcl-2 protein family. *Eur J Biochem*. 2001;268(5): 1352–1362.

40. James SA, Feltis BN, de Jonge MD, et al. Quantification of ZnO nanoparticle uptake, distribution, and dissolution within individual human macrophages. *ACS Nano*. 2013;7(12):10621–10635.

41. Johnson BM, Fraietta JA, Gracias DT, et al. Acute exposure to ZnO nanoparticles induces autophagic immune cell death. *Nanotoxicology*. 2015;9(6):737–748.

42. Xia T, Zhao Y, Sager T, et al. Decreased dissolution of ZnO by iron doping yields nanoparticles with reduced toxicity in the rodent lung and zebrafish embryos. *ACS Nano*. 2011;5(2):1223–1235.

43. George S, Pokhrel S, Xia T, et al. Use of a rapid cytotoxicity screening approach to engineer a safer zinc oxide nanoparticle through iron doping. *ACS Nano*. 2010;4(1):15–29.

44. Wang Y, Yuan L, Yao C, et al. A combined toxicity study of zinc oxide nanoparticles and vitamin C in food additives. *Nanoscale*. 2014;6(24): 15333–15342.

45. Xia T, Kovochich M, Liong M, et al. Comparison of the mechanism of toxicity of zinc oxide and cerium oxide nanoparticles based on dissolution and oxidative stress properties. *ACS Nano*. 2008;2(10):2121–2134.

46. Müller KH, Kulkarni J, Motskin M, et al. pH-dependent toxicity of high aspect ratio ZnO nanowires in macrophages due to intracellular dissolution. *ACS Nano*. 2010;4(11):6767–6779.

47. Huang CC, Aronstam RS, Chen DR, Huang YW. Oxidative stress, calcium homeostasis, and altered gene expression in human lung epithelial cells exposed to ZnO nanoparticles. *Toxicol In Vitro*. 2010; 24(1):45–55.

48. Karna P, Zughaier S, Pannu V, Simmons R, Narayan S, Aneja R. Induction of reactive oxygen species-mediated autophagy by a novel microtubule-modulating agent. *J Biol Chem*. 2010;285(24):18737–18748.

49. Rikiishi H. Novel insights into the interplay between apoptosis and autophagy. *Int J Cell Biol*. 2012;2012:317645.

50. Yu KN, Yoon TJ, Minai-Tehrani A, et al. Zinc oxide nanoparticle induced autophagic cell death and mitochondrial damage via reactive oxygen species generation. *Toxicol In Vitro*. 2013;27(4):1187–1195.

51. Roy R, Singh SK, Chauhan LK, Das M, Tripathi A, Dwivedi PD. Zinc oxide nanoparticles induce apoptosis by enhancement of autophagy via PI3K/Akt/mTOR inhibition. *Toxicol Lett*. 2014;227(1):29–40.

52. Saptarshi SR, Feltis BN, Wright PF, Lopata AL. Investigating the immunomodulatory nature of zinc oxide nanoparticles at sub-cytotoxic levels in vitro and after intranasal instillation in vivo. *J Nanobiotechnology*. 2015;13:6.

53. De Angelis I, Barone F, Zijno A, et al. Comparative study of ZnO and TiO$_2$ nanoparticles: physicochemical characterisation and toxicological effects on human colon carcinoma cells. *Nanotoxicology*. 2013;7(8): 1361–1372.

54. Guan R, Kang T, Lu F, Zhang Z, Shen H, Liu M. Cytotoxicity, oxidative stress, and genotoxicity in human hepatocyte and embryonic kidney cells exposed to ZnO nanoparticles. *Nanoscale Res Lett*. 2012; 7(1):602.

55. Kim AR, Ahmed FR, Jung GY, Cho SW, Kim DI, Um SH. Hepatocyte cytotoxicity evaluation with zinc oxide nanoparticles. *J Biomed Nanotechnol*. 2013;9(5):926–929.

56. Fukui H, Horie M, Endoh S, et al. Association of zinc ion release and oxidative stress induced by intratracheal instillation of ZnO nanoparticles to rat lung. *Chem Biol Interact*. 2012;198(1–3):29–37.

57. Kao YY, Chen YC, Cheng TJ, Chiung YM, Liu PS. Zinc oxide nanoparticles interfere with zinc ion homeostasis to cause cytotoxicity. *Toxicol Sci*. 2012;125(2):462–472.

58. Guo D, Bi H, Wu Q, Wang D, Cui Y. Zinc oxide nanoparticles induce rat retinal ganglion cell damage through Bcl-2, caspase-9 and caspase-12 pathways. *J Nanosci Nanotechnol*. 2013;13(6):3769–3777.

59. Xu F, Piett C, Farkas S, Qazzaz M, Syed NI. Silver nanoparticles (AgNPs) cause degeneration of cytoskeleton and disrupt synaptic machinery of cultured cortical neurons. *Mol Brain*. 2013;6:29.

60. Soenen SJ, Manshian B, Montenegro JM, et al. Cytotoxic effects of gold nanoparticles: a multiparametric study. *ACS Nano*. 2012;6(7): 5767–5783.

61. Wu J, Wang C, Sun J, Xue Y. Neurotoxicity of silica nanoparticles: brain localization and dopaminergic neurons damage pathways. *ACS Nano*. 2011;5(6):4476–4489.

62. Yang X, He C, Li J, et al. Uptake of silica nanoparticles: neurotoxicity and Alzheimer-like pathology in human SK-N-SH and mouse neuro2a neuroblastoma cells. *Toxicol Lett*. 2014;229(1):240–249.

63. Chen L, Yokel RA, Hennig B, Toborek M. Manufactured aluminum oxide nanoparticles decrease expression of tight junction proteins in brain vasculature. *J Neuroimmune Pharmacol*. 2008;3(4):286–295.

64. Apopa PL, Qian Y, Shao R, et al. Iron oxide nanoparticles induce human microvascular endothelial cell permeability through reactive oxygen species production and microtubule remodeling. *Part Fibre Toxicol*. 2009;6:1.

65. Lee CF, Liu CY, Hsieh RH, Wei YH. Oxidative stress-induced depolymerization of microtubules and alteration of mitochondrial mass in human cells. *Ann N Y Acad Sci*. 2005;1042:246–254.